An Alternative Cardinal Spline for Cubic B-Spline Interpolation

Juanjuan Chen, Qiumei Li, Junjuan Chen
School of Mathematics and Statistics
Guangxi Normal University
Guilin, China

Wei Qi Yan
Department of Computer and Information Sciences
Auckland University of Technology
Auckland, New Zealand

***Abstract*—This paper aims at introducing a special cubic cardinal spline from the GMK-splines, which is able to obtain almost the same interpolation results of the cubic B-spline, but without solving the system of equations for getting control vertices, and exploring its applications in geometric modeling and image processing. The spline involved can be obtained by using a linear combination of several shifted B-splines of the same degree. The spatial and frequency domain comparison demonstrates its superior local support and frequency domain performance. In addition, a number of examples are involved in geometric modeling and digital image processing, compared with a few conventional methods. As shown in this paper, the cubic cardinal spline is an alternative choice instead of the cubic B-spline in the interpolation procedure in order to avoid solving the system of equations over and over again.**

***Index Terms*—GMK-spline, B-spline, interpolation, geometric modeling, image processing.**

I. Introduction

Spline generally possesses a few merit properties, such as local shape control and high-order smoothness, with pretty rich applications, such as data fitting [1], [2], interpolation [3], sketching, curve and surface modeling. The earliest recorded use of splines in a manufacturing environment seems to go back to early AD Roman times for the purpose of ship building. With the advent of the big data era and artificial intelligence (AI), spline methods are still widely applied to multiple fields, i ncluding c omputer-aided g eometric design (CAGD) [4], [5], signal and image processing [6]–[13], industry manufacture, information science [14], [15], applied mathematics [16], engineering science and technology [17]–[19], and mechanical engineering [20]. Applications have led to decades of research for all types of spline functions, including polynomial splines [21], cardinal splines [22], [23], and rational splines. Especially, cardinal splines, also called explicit interpolatory splines, catch great interest from engineers and researchers and have a tremendous impact in these fields.

Among all the existing spline interpolation schemes, high-order B-splines play a crucial role in geometric modeling and digital image processing in which they can provide interpolation results of high-order smoothness which always means high quality. However, these high-order B-splines are not explicitly interpolatory, hence, there exists a troublesome problem that is to solve the system of equations in an interpolation procedure for getting control vertices. In order to overcome this problem, the B-spline interpolators are proposed by means of multiple signal processing techniques in the literature [23], [24].

Hence, the B-spline interpolators are the summations of infinite terms and are not exactly locally supported. However, this inspires the question whether there exist local-supported basis functions represented by a finite number of shifted B-splines? Therefore, we construct a class of basis functions. This idea is in accordance with the many-knots (abbreviated as MK)-spline, which was first proposed by Qi et al. [21]. Since the MK-spline is proposed, it has made a plethora of applications and great achievements [25]–[27].

In this paper, we introduce a special cubic cardinal spline that behaves like B-spline interpolation in applications like geometric modeling and image processing, but without solving equations for control vertices. This spline is a special generalized MK-spline (GMK-spline) with explicit interpolatory property. The GMK-spline, proposed in our prior work [28], has infinitely distinct basis functions. Similarly to the GMK-spline, the spline is also a linear combination of several same-degree shifted B-splines, with coefficients determined by solving Lagrange interpolation condition equations. It inherits cubic B-spline properties like central symmetry, local support, integral unity, partition of unity, and linear precision. It achieves interpolation without solving control vertex equations, and replaces cubic B-splines in interpolation, yielding nearly identical results in geometric modeling and image processing. To prove this, we compare it with cubic B-splines and the interpolators in spatial and frequency domains, and present examples in geometric modeling and image processing.

The subsequent structure of this paper is organized as follows. Section II constructs a special cardinal spline, firstly introducing the cubic B-spline basis function, then expounding the cardinal basis function representation of the GMK-spline, the solution of the equation system, and spatial and frequency analysis. Section III presents the applications of the spline in geometric modeling (curve and surface design) and image processing (low-pass frequency filter), together with method comparisons. Section IV summarizes the characteristics, advantages and application prospects of the GMK-spline.

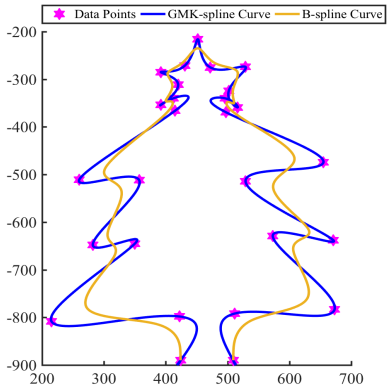

Fig. 1. Examples of GMK-spline curve and B-spline curve.

II. Cardinal spline construction

In this paper, we introduce a special cardinal spline from the GMK-spline [28] instead of the cubic B-spline in the interpolation procedure in order to avoid solving the system of equations over and over again.

When a spline basis function $s(t)$ satisfies the Lagrange interpolation conditions:

$$s(0) = 1,\ s(k) = 0,\ k \neq 0,\ k \in \mathbb{Z}, \tag{1}$$

where the spline $s(t)$ is called a cardinal spline or an explicit interpolatory spline, which is the basic definition for the subsequent construction of a cardinal spline.

A. Cubic B-spline basis function

Denote $\beta_3(t)$ as the cubic B-spline. Its algebraic representation is provided,

$$\beta_3(t) = \begin{cases} \frac{|t|^3}{2} - t^2 + \frac{2}{3}, & |t| \leq 1; \\ -\frac{|t|^3}{6} + t^2 - 2|t| + \frac{4}{3}, & 1 < |t| < 2; \\ 0, & |t| \geq 2, \end{cases} \tag{2}$$

In terms of piecewise polynomials with uniform knots, the cubic B-spline $\beta_3(t)$ in (2) has local support over $[-2, 2]$. We know that it has second smoothness at the knots. However, the cubic B-spline is not a cardinal spline and lacks explicit interpolatory. That is to say, for the B-spline interpolation, we need to determine the coefficients (or control vertices) so that the resulting function can pass through the given samples.

In the following, we briefly introduce a cubic B-spline interpolator, which is a basis function satisfying (1) and proposed in [23], [29], [30]. Based on the cubic B-spline, the B-spline interpolator is presented by

$$\eta_3(t) = \frac{-6\alpha}{1-\alpha^2} \sum_{k=-\infty}^{+\infty} \alpha^{|k|} \beta_3(t-k), \tag{3}$$

where the constant α equals $\sqrt{3} - 2$. The basis function $\eta_3(t)$ has the explicit interpolation property, but obviously, it has infinite terms and infinite support, which will lead to minor truncation errors. We use it in this work to explain the truth of cubic B-spline interpolation. Therefore, it is conceptual, but with little practical usefulness.

B. Cardinal basis function representation

Unlike the B-spline interpolator (3) whose shifts are all integers, the shifts for the GMK-spline basis functions are any real numbers. Additionally, since the GMK-spline is a cardinal (interpolatory) spline designed with central symmetry, its shifts must appear in pairs. For convenience, we sort the positive shifts in ascending order as $0 \leq a_1 < a_2 < \cdots < a_I$. Therefore, the basis functions of the GMK-spline are written in the form of convolution by

$$\begin{aligned} g(t) &= \sum_{i=1}^{I} A_i \frac{\beta_3(t+a_i) + \beta_3(t-a_i)}{2} \\ &= (A_1\delta_{a_1} + A_2\delta_{a_2} + \cdots + A_I\delta_{a_I}) * \beta_3(t), \end{aligned} \tag{4}$$

where A_i and a_i $(i = 1, 2, \cdots, I)$ are undetermined constants, and $\beta_3(t)$ is the cubic B-spline. In addition,

$$\delta_a(t) = \frac{\delta(t+a) + \delta(t-a)}{2},$$

where $\delta(t)$ is a Dirac delta function and the constant a is a time shift.

C. Equation system

To determine the unknown constants A_i and a_i $(i = 1, 2, \cdots, I)$, we start by simplifying the interpolation condition (1). The cubic B-spline $\beta_3(t)$ defined in (2) has a local support $[-2, 2]$. This means $\beta_3(t - a_I) \equiv 0$ when $t \geq a_I + 2$, and consequently, $g(n) \equiv 0$ for any integer n such that n $\geq \lceil a_I \rceil + 2$ (where $\lceil x \rceil$ represents the smallest integer greater than or equal to x). Therefore, under the interpolation condition (1), we only need to consider the cases where $n = 0, 1, \cdots, \lceil a_I \rceil + 1$. This leads to the following system of nonlinear equations with constraints $\lceil a_I \rceil + 2$:

$$\begin{cases} g(0) & = 1; \\ g(1) = g(2) = \cdots = g(\lceil a_I \rceil + 1) & = 0. \end{cases} \tag{5}$$

Since $\lceil a_I \rceil \geq 1$, the number of constraints is at least three. The equation system (5) implies that $\sum_{i=1}^{I} A_i = 1$ for any basis function $g(t)$. The detailed proof of this result is presented in [28].

In order to obtain the special cardinal spline, we select $a_1 = 0$, $a_2 = \frac{5}{4}$, $a_3 = \frac{7}{4}$, and $a_4 = 2$. The reason why we choose these shifts originates from deeper research is based on [28]. Then, we substitute them into equation (5). Next, the corresponding equation is simplified as follows:

$$\begin{bmatrix} \beta_3(0) & \beta_3(\frac{5}{4}) & \beta_3(\frac{7}{4}) & 0 \\ 2\beta_3(1) & \beta_3(\frac{1}{4}) & \beta_3(\frac{3}{4}) & \beta_3(1) \\ 0 & \beta_3(\frac{3}{4}) & \beta_3(\frac{1}{4}) & \beta_3(0) \\ 0 & \beta_3(\frac{7}{4}) & \beta_3(\frac{5}{4}) & \beta_3(1) \end{bmatrix} \begin{bmatrix} A_1 \\ A_2 \\ A_3 \\ A_4 \end{bmatrix} = \begin{bmatrix} 1 \\ 0 \\ 0 \\ 0 \end{bmatrix}. \tag{6}$$

This shows that the coefficient matrix is non-singular and the equation exists only one solution. Solving (6), we achieve $A_1 = \frac{130}{79}$, $A_2 = -\frac{1016}{711}$, $A_3 = -\frac{104}{79}$, and $A_4 = -\frac{379}{711}$.

D. Spatial and frequency analysis

That is to say, a cubic cardinal spline is represented as follows:

$$g(t) = \left(\frac{130}{79}\delta_0 - \frac{1016}{711}\delta_{\frac{5}{4}} + \frac{104}{79}\delta_{\frac{7}{4}} - \frac{379}{711}\delta_2\right) * \beta_3(t).$$

Its algebraic expression is obtained after computing a convolution of the B-spline basis function (2) and these shift operators. The algebraic expression is more efficient in practical applications. For convenience, the algebraic expression of the cubic cardinal spline is provided as:

$$g(t) = \begin{cases} \frac{6641}{8532}|t|^3 - \frac{478}{237}t^2 + 1, & |t| < \frac{1}{4}; \\ \frac{11641}{8532}|t|^3 - \frac{3493}{1422}t^2 + \frac{625}{5688}|t| + \frac{67631}{68256}, & \frac{1}{4} \le |t| < \frac{3}{4}; \\ \frac{6881}{8532}|t|^3 - \frac{854}{237}t^2 - \frac{2365}{2844}|t| + \frac{5231}{4266}, & \frac{3}{4} \le |t| < 1; \\ -\frac{107}{948}|t|^3 + \frac{123}{79}t^2 - \frac{3403}{948}|t| + \frac{339}{158}, & 1 \le |t| < \frac{5}{4}; \\ -\frac{2353}{2844}|t|^3 + \frac{1004}{237}t^2 - \frac{3289}{948}|t| + \frac{40283}{11376}, & \frac{5}{4} \le |t| < \frac{7}{4}; \\ -\frac{481}{2844}|t|^3 + \frac{185}{79}t^2 - \frac{845}{948}|t| + \frac{19}{1422}, & \frac{7}{4} \le |t| < 2; \\ -\frac{51}{316}|t|^3 + \frac{58}{79}t^2 - \frac{757}{948}|t| - \frac{23}{474}, & 2 \le |t| < \frac{9}{4}; \\ \frac{2687}{8532}|t|^3 - \frac{196}{79}t^2 + \frac{6101}{948}|t| - \frac{10379}{1896}, & \frac{9}{4} \le |t| < \frac{11}{4}; \\ -\frac{1057}{8532}|t|^3 + \frac{90}{79}t^2 - \frac{3337}{948}|t| + \frac{577}{158}, & \frac{11}{4} \le |t| < 3; \\ \frac{17}{316}|t|^3 - \frac{109}{237}t^2 + \frac{1211}{948}|t| - \frac{181}{158}, & 3 \le |t| < \frac{13}{4}; \\ -\frac{557}{8532}|t|^3 + \frac{997}{1422}t^2 - \frac{14197}{5688}|t| + \frac{200827}{68256}, & \frac{13}{4} \le |t| < \frac{15}{4}; \\ \frac{379}{8532}(|t| - 4)^3, & \frac{15}{4} \le |t| < 4; \\ 0, & \text{otherwise.} \end{cases}$$

When we choose different n, I and h, various basis functions of the GMK-spline are derived. Fig. 1 shows the results using the GMK-spline and the B-spline, where we do not solve systems of equations. We found that the GMK-spline curve passes through each given data point, whereas the B-spline curve cannot pass through them. The plots of several special splines are shown in Fig. 2. It is clear that the GMK-spline $g(t)$ has compact support interval over $[-4, 4]$, but the B-spline interpolator has not strictly local support; the GMK-spline has better frequency performance than the B-spline and is even better a little bit than the B-spline interpolator in the sense of approximating the idea filter.

For convenience, Fourier transforms of the cubic B-spline, the cubic B-spline interpolator (3), and the special cubic GMK-spline $g(t)$ are given as:

$$H_{\mathrm{B}}(\omega) = \begin{cases} \left(\frac{2\sin(\omega/2)}{\omega}\right)^4, & \omega \neq 0; \\ 1, & \omega = 0, \end{cases} \tag{7}$$

$$H_{\mathrm{Bint}}(\omega) = \begin{cases} \frac{48\sin^4(\omega/2)}{\omega^4(2+\cos(\omega))}, & \omega \neq 0; \\ 1, & \omega = 0, \end{cases} \tag{8}$$

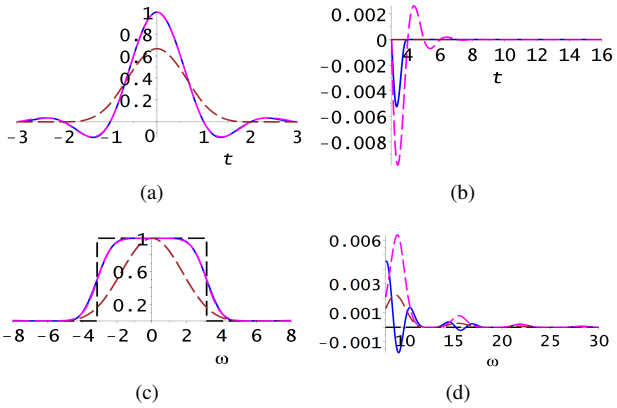

Fig. 2. Comparison among the three different basis functions: Cubic B-spline (brown dotted solid line), cubic B-spline interpolator $\eta_3(t)$ (magenta dotted line), and the GMK-spline $g(t)$ (blue solid line). (a) Comparison in spacial domain, where cubic B-spline interpolator refers to a truncation of $\eta_3(t)$ in (3) with $k = -200, \ldots, 200$ and $t \in [-3, 3]$. (b) Comparison in spacial domain, where $t \in [3, 16]$. (c) Comparison in frequency domain, adding the ideal filter (black dash line), where $\omega \in [-8, 8]$. (d) Comparison in frequency domain, where $\omega \in [8, 30]$.

$$H_{\mathrm{g}}(\omega) = \begin{cases} \frac{-16\left(\sin\left(\frac{\omega}{2}\right)\right)^4}{711\omega^4} \cdot P(\omega), & \omega \neq 0; \\ 1, & \omega = 0, \end{cases} \tag{9}$$

where

$$\begin{aligned} P(\omega) = {} & 48512\cos^8\left(\frac{\omega}{4}\right) - 59904\cos^7\left(\frac{\omega}{4}\right) \\ & - 97024\cos^6\left(\frac{\omega}{4}\right) + 121088\cos^5\left(\frac{\omega}{4}\right) \\ & + 60640\cos^4\left(\frac{\omega}{4}\right) - 72736\cos^3\left(\frac{\omega}{4}\right) \\ & - 12128\cos^2\left(\frac{\omega}{4}\right) + 11632\cos\left(\frac{\omega}{4}\right) - 791. \end{aligned}$$

III. Applications in Geometric Modeling and Image Processing

In [31], the GMK-spline has multiple beneficial properties, such as explicit interpolation, strict local support, high-order smoothness, unity of integral, partition of unity, and linear precision. Of course, different GMK-splines have various interpolation effects. In this paper, we focus only on one special GMK-spline. By using this spline, one can easily construct various curves and surfaces from just a few sample points. So, designs based on it offer a high degree of predictability and freedom. A few examples of shape design by using the GMK-spline are presented. Note that we employ parametric expressions to overcome the problem of non-uniform sampling.

A. Curve design

A curve passing through a set of given data points $P_k \in \mathbb{R}^d$ (the dimension $d \geq 2$) is represented as

$$P(t) = \sum_k P_k g(t - k), \tag{10}$$

with the basis functions of the GMK-spline. Then, the interpolatory curve has C^2-continuity. This interpolation equation

(10) is explicit in terms of the input discrete data $\{P_k\}$. We choose $d = 2$ as an example and suppose $P_k = (x_k, y_k)$, thus, we get the resulting planar curve in the parameter form as below:

$$\begin{cases} x(t) = & \sum_k x_k g(t-k); \\ y(t) = & \sum_k y_k g(t-k). \end{cases}$$

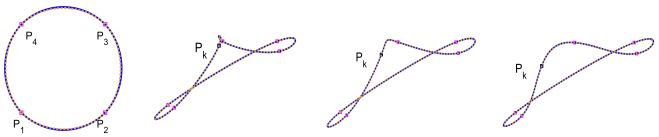

(a) (b) (c) (d)

Fig. 3. Closed curve construction using cubic GMK-splines $g(t)$ (blue solid line), and cubic B-spline (brown dotted line). (a) The interpolatory curve produced by using repeatedly some points three times to approximate a circle. (b) The sample point P_k is very close to the next one, that results in a knot on the resulting curve. (c) Modify the position of P_k to eliminate the knot. (d) Further modify the position of P_k to get more beautiful curve shape.

Based on this parameter form, the examples related to surface design are given in the following. Taking into account four vertices of a square and one connecting point from them, these five points are queued clockwise or counterclockwise as the original sample points, i.e. P_1, P_2, P_3, P_4, P_1, where P_1 is called the connecting point. For $n \geq 2$, the interpolatory curves closely approximate a circle by repeatedly using the endpoints a number of times. Within this example, the sequence of the control points used is listed as follows:

$$P_3,\ P_4,\ P_1,\ P_2,\ P_3,\ P_4,\ P_1,\ P_2,\ P_3. \tag{11}$$

Hence, it produces a closed curve that is very close to a circle. These control points of this example are given specifically as $P_1 = (0, 0)$, $P_2 = (2, 0)$, $P_3 = (2, 2)$, and $P_4 = (0, 2)$. In addition, the approximated circle is with the center of $(1, 1)$ and the radius of $\sqrt{2}$. As shown in Fig. 3 (a). Interestingly, by adjusting the position of P_k, the shape of the curve is also locally modified. This local modification feature is very flexible. In practical applications, when fine adjustment of a specific local area of the curve is necessary to meet specific shape requirements, only the position of P_k needs to be changed in a targeted manner, without making large-scale adjustments to the control points of the entire curve, providing convenience for personalized design and optimization of the curve. As shown in Fig. 3 (b)-(d).

In the following, the related rules are summarized for basic shape curves.

- **Open curves**: The shape of an open curve is affected by the number of sample points and the repetition times of the endpoints. The repetition times of the endpoints should match the support interval of the basis function. For example, for $g(t)$ with a support interval of [-4, 4], its endpoints usually need to be repeated four times.
- **Closed curves**: Select appropriate sample points (such as square vertices combined with a connecting point), and the curve can be approximated to a circle by repeating the endpoints. If initial sampling causes an unsatisfactory result, the curve is optimized by resampling, inserting additional points, and locally adjusting one or several samples, as shown in Fig. 3 (b)-(d).
- **Spline comparison**: As shown in Fig. 4, compared to cubic B-spline fitting and linear interpolation, the GMK-spline performs significantly better in the spatial domain and has an interpolation result very similar to the B-spline interpolation, making it an excellent alternative.

B. Surface design

A tensor surface passing through a grid of given data points $\{P_{ij}\}$ ($P_{ij} \in \mathbb{R}^d$, the dimension $d \geq 3$) is represented in the parameter form:

$$P(t_1, t_2) = \sum_i \sum_j P_{ij} g(t_1 - i) g(t_2 - j),$$

Using the GMK-spline basis function $g(t)$, the interpolatory surface then has C^2-continuity. Note that the given data are required to be regular or on the grid. Taking $d = 3$ into consideration for general applications and assuming $P_{ij} = (x_{ij}, y_{ij}, z_{ij})$, we get the resulting surface $P = (x, y, z)$ as follows:

$$\begin{cases} x(t_1, t_2) = & \sum_i \sum_j x_{ij} g(t_1 - i) g(t_2 - j); \\ y(t_1, t_2) = & \sum_i \sum_j y_{ij} g(t_1 - i) g(t_2 - j); \\ z(t_1, t_2) = & \sum_i \sum_j z_{ij} g(t_1 - i) g(t_2 - j). \end{cases}$$

The control points in (11) are 2D. Now, they are extended to the 3D space: $P_1 = (0, 0, 0)$, $P_2 = (2, 0, 0)$, $P_3 = (2, 2, 0)$, and $P_4 = (0, 2, 0)$, and two other control points are added to them: $P_5 = (1, 1, -\sqrt{2})$ and $P_6 = (1, 1, \sqrt{2})$. The corresponding control grid is given as

$$\begin{bmatrix} P_1 & P_1 & P_1 & P_1 & P_1 \\ P_2 & P_5 & P_4 & P_6 & P_2 \\ P_3 & P_3 & P_3 & P_3 & P_3 \\ P_4 & P_6 & P_2 & P_5 & P_4 \\ P_1 & P_1 & P_1 & P_1 & P_1 \end{bmatrix},$$

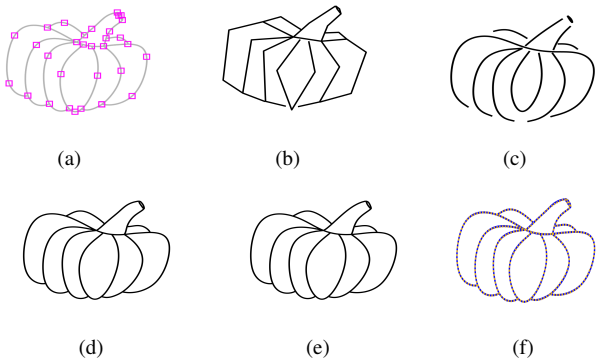

(a) (b) (c) (d) (e) (f)

Fig. 4. Shape design example. (a) Sample points. (b) Linear interpolation. (c) Cubic B-spline fitting. (d) Cubic GMK-spline interpolation by $g(t)$. (e) Cubic B-spline interpolation. (f) Comparison among the GMK-splines $g(t)$ (blue solid line) and the cubic B-spline (brown dotted line).

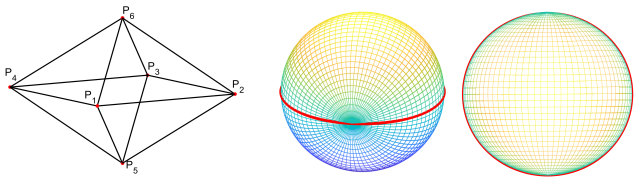

(a) (b) (c)

Fig. 5. (a) Control polygon. (b) GMK-spline $g(t)$ surface. (c) GMK-spline $g(t)$ surface.

where there are only six distinct control points from the control polygon shown in Fig. 5 (a) The resulting surfaces approximate a ball centered at $(1, 1, 0)$ with radius $\sqrt{2}$, provided that the grid is extended by repeating the control points in a manner similar to that described in (11). Based on the extended grid, the surface of the GMK-spline generated by $g(t)$ very closely approximates the target ball, as shown in Fig. 5 (b) and (c).

C. Digital Image processing

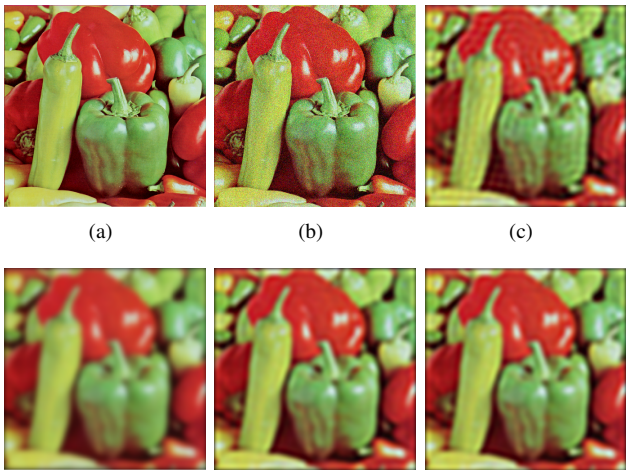

(a) (b) (c)

(d) (e) (f)

Fig. 6. Comparison of image processing: (a) Original image; (b) Image polluted by Gaussian noise of $\mu = 0$ and $\sigma = 0.01$; (c) Image denoising by ideal filter; (d) Image denoising by cubic B-spline (7); (e) Image denoising by B-spline interpolator (8); (f) Image denoising by GMK-spline $H_g(\omega)$ (9).

The GMK-spline is applied to image denoising. For a noisy image $f(x, y)$ corrupted by Gaussian noise, we firstly cope it with $(-1)^{x+y}$, then compute its Fourier transform $F(u, v)$. Next, multiply $F(u, v)$ by the filter transfer function in the frequency domain $H(u, v)$ based on different frequency functions to obtain

$$\tilde{F}(u, v) = H(u, v) \cdot F(u, v).$$

Afterwards, we perform an inverse Fourier transform on $\tilde{F}(u, v)$, extract the real part, and perform post-processing with $(-1)^{x+y}$ to obtain the denoised image $\tilde{f}(x, y)$.

We set the variable ω in the frequency functions (7)-(9) for low-pass filters as:

$$\omega = \pi \frac{D(u, v)}{D_0},$$

and for high-pass filters as:

$$\omega = \pi \frac{D_0}{D(u, v)},$$

where D_0 is the cutoff frequency, $D(u, v)$ is the distance from a point (u, v) in the frequency plane to the center. If the image size is $M \times N$, the corresponding array center is $\left(\frac{M}{2}, \frac{N}{2}\right)$, then

$$D(u, v) = \sqrt{(u - \frac{M}{2})^2 + (v - \frac{N}{2})^2}. \tag{12}$$

To further verify the effectiveness of the GMK-spline-based frequency domain filter in image denoising, visual and quantitative evaluations are conducted. As we see from TABLE I and Fig. 6, for different test images (such as peppers, portrait, Milk Drop Coronet, scenery, etc.) contaminated by Gaussian noise with the same mean value ($\mu = 0$) and different variances (σ^2 = $0.1, 0.01, 0.001$):

Although the ideal low-pass filter (Fig. 6 (c)) achieves a relatively moderate PSNR under multiple variances, its visual quality is impaired due to the Gibbs phenomenon; the cubic B-spline filter (Fig. 6 (d)) has the problem of excessive smoothing, leading to serious loss of fine details in the image, and its PSNR is relatively low; the B-spline interpolator (Fig. 6 (e)) has a reasonable PSNR performance (e.g., 22.39 dB when $\sigma^2 = 0.01$); however, in contrast, the GMK-spline filter (Fig. 6 (f)) shows competitiveness in various images and noise variances. Taking the pepper image in Fig. 6 with $\sigma^2 = 0.01$ as an example, its PSNR reaches 22.40 dB, and SSIM is 0.9119, which is higher than 0.9067 of the ideal low-pass filter, 0.8826 of the cubic B-spline filter, and even slightly better than 0.9117 of the B-spline interpolator.

With excellent frequency characteristics, the GMK-spline-based filters effectively suppress Gaussian noise in specific frequency regions, ensuring that the denoised image retains natural details without excessive smoothing. In different test images and different noise variance scenarios, its visual effect and quantitative indicators (PSNR, SSIM) are superior to the aforementioned various filters.

IV. Conclusion

In conclusion, the cubic cardinal spline proposed in this paper is an efficient alternative to the cubic B-spline and is a special spline from the cubic GMK-splines. It inherits the excellent properties of the B-spline like central symmetry and local support, while possessing explicit interpolation capability without the need for additional solution of systems of equations. The spatial and frequency domain comparison demonstrates its superior local support and frequency domain performance. Geometric modeling examples are applied to verify that it is able to construct high-precision and high-smoothness shapes with a small number of sampling points, and the endpoint repetition strategy adapts to the requirements of both open and closed graphics. In image denoising, the frequency-domain filter based on this spline is able to effectively suppress Gaussian noise, balance the denoising effect and detail preservation, and avoid over-smoothing. Therefore,

TABLE I
PSNR AND SSIM RESULTS OF DIFFERENT IMAGES AND FILTERS

Image	Variance	Ideal Lowpass Filter		B-spline Filter		B-spline interpolator Filter		GMK-spline Filter	
		PSNR (dB)	SSIM	PSNR (dB)	SSIM	PSNR (dB)	SSIM	PSNR (dB)	SSIM
	0.1	20.49	0.8627	19.09	0.8409	20.65	0.8670	20.66	0.8672
	0.01	22.04	0.9067	20.47	0.8826	22.39	0.9117	22.40	0.9119
	0.001	22.13	0.9109	20.57	0.8865	22.49	0.9160	22.50	0.9162
	0.1	20.70	0.6952	19.72	0.7528	20.94	0.7273	20.94	0.7269
	0.01	22.57	0.8171	20.90	0.8244	22.85	0.8460	22.87	0.8463
	0.001	22.82	0.8335	21.04	0.8320	23.12	0.8631	23.13	0.8635
	0.1	21.53	0.8732	20.22	0.8606	21.63	0.8783	21.64	0.8784
	0.01	24.12	0.9121	22.13	0.8951	24.45	0.9181	24.46	0.9183
	0.001	24.22	0.9159	22.23	0.8986	24.58	0.9221	24.60	0.9222
	0.1	18.91	0.6818	17.87	0.6549	19.08	0.6936	19.09	0.6937
	0.01	19.80	0.7448	18.78	0.7152	20.11	0.7578	20.12	0.7579
	0.001	19.83	0.7490	18.81	0.7192	20.15	0.7621	20.15	0.7622

this proposed spline has important theoretical value and application potential in computer-aided geometric design, signal and image processing. The focus of our future research work is on exploring the application in higher-dimensional data processing and complex dynamic modeling.

REFERENCES

[1] G. Farin, *Curves and Surfaces for Computer Aided Geometric Design: A Practical Guide*, 4th ed. USA: Academic Press, 1997.

[2] W. Yan and D. Qi, "Rational many-knot spline interpolating curves and surfaces," *Journal of Image and Graphics*, vol. 6, no. 6, pp. 568–572, 2001.

[3] S. Okaniwa, A. Nasri, H. Lin, A. Abbas, Y. Kineri, and T. Maekawa, "Uniform B-spline curve interpolation with prescribed tangent and curvature vectors," *IEEE Transactions on Visualization and Computer Graphics*, vol. 18, no. 9, pp. 1474–1487, September 2012.

[4] J. J. Chen and F. F. Peng, "Approximate spline of G^2-continuity on a generalized hyperbolic paraboloid," *Journal of Computational and Applied Mathematics*, vol. 248, no. 2, pp. 99–117, 2013.

[5] G. Albrecht, C. V. Beccarib, J.-C. Canonne, and L. Romani, "Planar Pythagorean-Hodograph B-spline curves," *Computer Aided Geometric Design*, vol. 248, no. 2, pp. 99–117, 2013.

[6] S. Lu, Y. Shen, and Y. Wang, "Generalized high-precision simulation for TT&C channels using B-spline signal processing," *IEEE Signal Processing Letters*, vol. 24, no. 9, pp. 1383–1387, September 2017.

[7] J. Pedrosa, S. Queirós, O. Bernard, and J. Engvall, "Fast and fully automatic left ventricular segmentation and tracking in echocardiography using shape-based B-spline explicit active surfaces," *IEEE Transactions on Medical Imaging*, vol. 36, no. 11, pp. 2287–2296, November 2017.

[8] H. Behjat, Z. Doğan, D. V. D. Ville, and L. Sörnmo, "Domain-informed spline interpolation," *IEEE Transactions on Signal Processing*, vol. 67, no. 15, pp. 3909–3921, August 2019.

[9] A. Daniyan, S. Lambotharan, A. Deligiannis, Y. Gong, and W.-H. Chen, "Bayesian multiple extended target tracking using labeled random finite sets and splines," *IEEE Transactions on Signal Processing*, vol. 66, no. 22, pp. 6076–6091, November 15 2018.

[10] J. Chen and Z. Cai, "Cardinal MK-spline signal processing: Spatial interpolation and frequency domain filtering," *Information Sciences*, vol. 495, pp. 116–135, 2019.

[11] J. Horváth and G.-M. Su, "Novel image super-resolution and denoising using implicit tensor-product B-spline," in *IS&T International Symposium on Electronic Imaging 2024: Image Processing: Algorithms and Systems XXII*, 2024, pp. 254–1 – 254–7.

[12] T. Lan, Z. Cai, and B. Ye, "A novel spline algorithm applied to COVID-19 computed tomography image reconstruction," *IEEE Transactions on Industrial Informatics*, vol. 18, no. 11, pp. 7804–7813, November 2022.

[13] W. Yan and D. Qi, "Many-knot spline interpolating curves and their applications in font design," *Computer Aided Drafting, Design and Manufacturing*, pp. 1–8, 1999.

[14] M. Gaeta, V. Loia, and S. Tomasiello, "Cubic B-spline fuzzy transforms for an efficient and secure compression in wireless sensor networks," *Information Sciences*, vol. 339, pp. 19–30, 2016.

[15] X. Zhao, C. Zhang, L. Xua, B. Yang, and Z. Feng, "IGA-based point cloud fitting using B-spline surfaces for reverse engineering," *Information Sciences*, vol. 245, pp. 276–289, 2013.

[16] M. KashifIqbal, M. Abbas, and I. Wasim, "New cubic B-spline approximation for solving third order Emden–Flower type equations," *Applied Mathematics and Computation*, vol. 331, no. 15, pp. 319–333, August 2018.

[17] J. Jauch, F. Bleimund, S. Rhode, and F. Gauterin, "Recursive B-spline approximation using the Kalman filter," *Engineering Science and Technology, an International Journal*, vol. 2017, no. 20, pp. 28–34, 2017.

[18] F. Sun and Z. Cai, "Cubic polishing spline-based algorithms for industrial image processing," *IEEE Transactions on Industrial Informatics*, vol. 20, no. 1, pp. 314–326, January 2024.

[19] T. Lan and Z. Cai, "Efficient reconstruction of industrial images using optimized HMK splines," *IEEE Transactions on Industrial Informatics*, vol. 17, no. 7, pp. 4657–4667, July 2021.

[20] S. Sun, D. Yu, C. Wang, and C. Xie, "A smooth tool path generation and real-time interpolation algorithm based on B-spline curves," *Advances in Mechanical Engineering*, vol. 10, no. 1, pp. 1–14, 2018.

[21] D. X. Qi, "On cardinal many-knot δ-spline interpolation (I)," *Acta Scientiarum Natur. Universitatis Jilinensis*, vol. 3, pp. 70–81, 1975.

[22] K. Hamm and J. Ledford, "Cardinal interpolation with general multiquadrics," *Advances in Computational Mathematics*, vol. 42, p. 1149–1186, 2016.

[23] M. Unser, "Splines a perfect fit for signal and image processing," *IEEE Signal Processing Magazine*, vol. 16, no. 6, pp. 22–38, November 1999.

[24] M. Unser, A. Aldroubi, and M. Eden, "Fast B-spline transforms for continuous image representation and interpolation," *IEEE Transactions on Pattern Analysis and Machine Intelligence*, vol. 13, no. 3, pp. 277–285, March 1991.

[25] W. Yan and M. Kankanhalli, "Detection and removal of lighting and shaking artifacts in home videos," *ACM International Conference on Multimedia*, pp. 107–116, 2002.

[26] D. Qi, R. Song, and J. Li, *Discontinuous Orthogonal Functions — U-Systems, V-Systems, Multiwavelets and Their Applications*. Beijing China: Science Press, 2011.

[27] W. Yan, *Robotic Vision: From Deep Learning to Autonomous Systems*. Singapore: Springer, 2025.

[28] J. Chen and Z. Cai, "A new class of explicit interpolatory splines and related measurement estimation," *IEEE Transactions on Signal Processing*, vol. 68, no. 1, pp. 2799–2813, December 2020.

[29] M. Unser, A. Aldroubi, and M. Eden, "B-spline signal processing: Part I–Theory," *IEEE Transactions on Signal Processing*, vol. 41, no. 2, pp. 821–833, February 1993.

[30] J. Zhang, "Two different forms of C-B-splines," *Computer Aided Geometric Design*, vol. 14, no. 1, pp. 31–41, January 1997.

[31] J. Chen and Z. Cai, "A new class of explicit interpolatory splines and related measurement estimation," *IEEE Transactions on Signal Processing*, vol. 68, p. 2799, August 2020.